Accepted Manuscript

Electrogenerated hydrophilic carbon nanomaterials with tailored electrocatalytic activity

S.G. Meirinho, A.M. Ferraria, A.M. Botelho do Rego, A.J.S. Fernandes, A.S. Viana, M.C. Oliveira

PII: S0013-4686(19)30250-6

DOI: https://doi.org/10.1016/j.electacta.2019.02.025

Reference: EA 33616

To appear in: *Electrochimica Acta*

Received Date: 6 November 2018

Revised Date: 5 January 2019

Accepted Date: 5 February 2019

Please cite this article as: S.G. Meirinho, A.M. Ferraria, A.M. Botelho do Rego, A.J.S. Fernandes, A.S. Viana, M.C. Oliveira, Electrogenerated hydrophilic carbon nanomaterials with tailored electrocatalytic activity, *Electrochimica Acta* (2019), doi: https://doi.org/10.1016/j.electacta.2019.02.025.

ELECTROGENERATED HYDROPHILIC CARBON NANOMATERIALS WITH TAILORED ELECTROCATALYTIC ACTIVITY

S. G. Meirinho[1], A. M. Ferraria[2], A. M. Botelho do Rego[2], A. J. S. Fernandes[3], A. S. Viana[4], M. C. Oliveira[*1]

[1]*CQ-VR, Dep. Química, Univ. de Trás-os-Montes e Alto Douro, 5000-801 Vila Real, Portugal*

[2]*CQFM and IN and IBB, Instituto Superior Técnico, Univ. de Lisboa, 1049-001 Lisboa, Portugal*

[3]*I3N, Dep. Física., Univ. de Aveiro, Campus de Santiago, 3810-193, Aveiro, Portugal*

[4]*CQB, CQE, Dep. Química e Bioquímica, Fac. de Ciências, Univ. de Lisboa, 1749-016 Lisboa, Portugal*

* corresponding author: mcris@utad.pt

Abstract

This work investigates the influence of the type of buffer electrolyte used in the generation of Electrochemical Hydrophilic Carbon (EHC) on their physical-chemical properties and electrocatalytic activity. The EHC nanomaterials were prepared in three different biological buffers, phosphate, glycine and citrate buffers (EHC@phosphate, EHC@glycine, EHC@citrate) and their surface properties were fully characterized by AFM, XPS and Raman. The EHC nanomaterials drop cast onto a glassy carbon electrode were electrochemically characterized in $[Fe(CN)_6]^{3-/4-}$ and $[Ru(NH_3)_6]^{3+/2+}$ redox probes solutions, and their electrocatalytic activity was investigated towards hydrogen peroxide and oxygen reduction reactions (ORR) in a phosphate buffer solution. It was found that the nature of buffer electrolyte strongly influences the surface chemical state of the EHC materials, disorder degree in the hexagonal sp^2 carbon network and oxygen functional groups, affecting both the EHC electrocatalytic activity towards the ORR and H_2O_2 reduction reaction. The most catalytic material for the ORR was EHC@citrate, whereas EHC@glycine showed the highest oxygen conversion ($n \cong 2.7$ to 3). Moreover, it was shown that the content of oxygen singly bonded to carbon correlates strongly with the number of electrons transferred.

A very singular behaviour in the electrochemical reduction of hydrogen peroxide was observed on EHC@glycine, qualitatively interpreted as an autocatalytic reaction. In contrast, a blocking-like effect was depicted on EHC@phosphate. These results must have an important impact in the development of materials with peroxidase-like activity and in the design of O_2 sensors with non-sensitivity to H_2O_2.

Keywords: electrocatalysis; oxygen reduction; peroxide reduction; hydrophilic carbon; autocatalysis.

1. Introduction

There is much interest in knowing how to modulate the properties of carbon nanomaterials using soft experimental approaches. Recently, one-pot and soft chemical procedure to generate a low-cost carbon-based nanomaterial in both cathodic and anodic sides of an electrochemical cell, was reported [1,2]. This material was named Electrogenerated Hydrophilic Carbon (EHC) due to its outstanding solubility in water. It was found that the EHC nanomaterial possesses a structure dominated by sp^2 carbons in a non-ordered carbon network formed by small clusters of a carbonaceous material. Plus, it was shown that the generated carbon-based material was able to form a bi-dimensional nanostructured layer with conductive properties, enabling its use as a thin film electrode material. It was demonstrated that the chemical and electrochemical properties of the carbon-based material released in the anodic compartment were different from those generated in the cathodic compartment [1,3]. For example, although both EHC films have shown good ability towards oxygen and hydrogen peroxide electrochemical reduction, the sensing capability was significantly better for the EHC produced in the anodic compartment than for the EHC released in the cathode side [3]. Following up these findings, this works aims to investigate if the electrolyte composition used in the electrochemical synthesis of EHC is also able to tune its physical-chemical and electrocatalytic properties. For this purpose, the EHC nanomaterial was generated at the anode in three different electrolyte solutions, phosphate (EHC@phosphate), citrate (EHC@citrate) and glycine (EHC@glycine) buffers. These electrolytes are representative of three different types of biological buffers (phosphate as an inorganic physiological buffer, citrate as a carboxylic acid buffer and glycine as an amino acid buffer) envisaging possible applications of the as-prepared EHC nanomaterials in the biomedical field. Afterwards, the nanomaterial was deposited on a glassy carbon electrode and its electrochemical behaviour was appraised in the neutral medium for two most important electrocatalytic reactions, the electrochemical reduction of hydrogen peroxide and the oxygen reduction reaction (ORR).

The electrocatalytic reduction of H_2O_2 is a topic that attracts much attention because of the wide range of implications in chemical and biochemical reactions. One of the main purposes of the research on the peroxide electrochemical reduction is the development of materials for rapid and accurate diagnostic tests in clinical applications (e.g. biosensing of glucose and cholesterol). In this field, carbon-based nanomaterials are very attractive because they are biocompatible and usually show peroxidase-mimicking activity, enabling the sensible and selective detection of H_2O_2. However, for therapeutic applications its use is still highly restrictive because the majority of carbon nanomaterials are not soluble in water [4]. Hence, EHC appear as a potential nanomaterial, whose behaviour can be appraised, in a first approach, by voltammetric techniques in a peroxide containing solution. Investigation, in neutral medium, of the ORR on carbon based materials is also an important topic, for example, to unravel catalase type enzymes, develop biocompatible oxygen sensors or cathode materials for Microbial Fuel cells.

2. Experimental

2.1 Synthesis: EHC nanomaterials were prepared according to the procedure previously described [1]. Briefly, one hour of galvanostatic polarization (I = 60 mA) was undertaken in a citrate buffer (pH = 6.5), phosphate buffer (pH = 7.0) or glycine buffer solutions (pH = 9.5) using graphite rods as anode and cathode. The electrochemical synthesis was performed under air atmosphere. Afterwards, the solution from the anodic compartment was removed and dialyzed with a 3.5-5 kDa molecular weight cut-off membrane.

2.2 Electrochemical characterization: The electrochemical characterization was performed in a 0.1 M phosphate buffer solution (PB) prepared from KH_2PO_4 and HK_2PO_4 chemicals. The EHC nanomaterial was cast onto a glassy carbon electrode (RDE, 3 mm in diameter), by dropping 20 µl of the dialysed EHC solution onto a polished surface, which dried slowly in air. This

procedure led to a carbon loading of 3.05, 2.17 and 4.80 μg cm^{-2} of EHC@phosphate, EHC@glycine and EHC@citrate, respectively. The carbon content was determined by Total Organic Carbon (TOC) analysis.

The electrochemical cell was assembled with the modified glassy carbon working electrode, an Ag/AgCl (KCl 3 M) reference electrode and a Pt mesh. Deaeration was achieved by bubbling high purity argon through the electrolyte for 20 min and the gas was maintained over the surface of the solution during the electrochemical experiments.

For the ORR experiments, the electrolyte solution was saturated with high purity O_2 by bubbling it for at least 30 min and a gentle oxygen flow was maintained above the cell solution. Measurements on the rotating disk electrode were carried out on a Pine electrode rotator with a Radiometer speed control unit from Autolab. The ORR polarization curves were obtained from the open circuit potential value (≅ 0.05 V) to -1.20 V at 20 mV s^{-1}, in a rotation range of 400 – 2100 rpm. All polarization curves were corrected for an uncompensated resistance of 197, 195 and 100 Ω for EHC@phosphate, EHC@glycine and EHC@citrate films, respectively, which were determined from electrochemical impedance spectroscopy. A Gamry Instruments Interface 1000E potentiostat was used to register impedance spectra from 100 kHz to 0.100 Hz with an amplitude of 15 mV. The impedance diagrams were interpreted with ZView software (Scribner, Inc.). The intercept with real axis (zero phase angle) was taken as the cell resistance.

Voltammetric curves for ORR were plotted as *j*–E where *j* is the current density normalized to the geometric area of the rotating disk electrode (0.07067 cm^2). All of the potentials are given with respect to the Ag/AgCl reference electrode.

Unless otherwise stated, the electrochemical reduction of H_2O_2 was carried out in an O_2-free solution containing 6.2 mM H_2O_2, obtained by the addition of 35 μL of 30 % w/v H_2O_2 to 50 mL of phosphate buffer solution. The cyclic voltammograms were recorded on an Autolab PGSTAT

100 potentiostat. All the electrochemical measurements were carried out at room temperature (≅ 20 ^{0}C).

2.3 Physicochemical Characterization: The EHC films were characterized by AFM, Raman and XPS. Atomic force microscopy was carried out in a Multimode 8 HR coupled to Nanoscope V, produced by Bruker, using Peak Force Tapping mode under ScanAsyst Control. Measurements were performed by placing a drop (ca. 30 µL) of each EHC sample onto freshly cleaved mica for 30 min and drying with pure N_2. The images were acquired in ambient conditions (ca. 21 ºC), using etched silicon tips with a spring constant of ca. 0.4 N/m (SCANASYST-AIR, Bruker), at a scan rate of ca. 1 Hz.

Raman spectroscopy was performed on EHC samples cast onto quartz slides. A confocal instrument in the backscatting configuration (Horiba HR800, Japan) was used under the excitation of the 441.6 nm line of a HeCd laser (Kimmon IK Series, Japan). The spectra were collected using a 100X objective (spot size 1-2 µm, NA = 0.9, Olympus, Japan), a 600 lines/mm grating and a multichannel back-thinned CCD detector, Peltier cooled to 203 K. For each spectrum, the selected integration time was 1 sec with 10 accumulations, while the confocal iris was set to 200 µm. The data treatment consisted in the background removal based on the Raman response of the substrate followed by band fitting with Gauss-Lorentzian functions, using the native Labspec software.

XPS analysis was performed using a non-monochromatic dual anode XSAM800 spectrometer from KRATOS. Sample preparation, spectrometer operating conditions and spectra acquisition parameters were described elsewhere [1,2]. Source satellites and Shirley backgrounds were subtracted from spectra. No flood gun was used for charge correction. The charge shift was corrected using, as reference, the C 1s binding energy (BE) of aliphatic carbon atoms centered at 285.0 eV. The sensitivity factors, used for quantification purposes, were those of software libraries.

3. Results and Discussion

3.1 Physicochemical characterization

AFM of EHC nanomaterials deposited on mica provide information about the surface morphology and roughness of the deposited films, **Figure 1**. AFM images and cross-sectional analyses show that all deposited films are formed by rounded grains with similar size and a slight porosity. The morphology of EHC@glycine films is strikingly smoother than the other two EHC materials investigated. On EHC@glycine film, the grains are densely and tightly packed, whereas on EHC@citrate and EHC@phosphate the grains are assembled on the surface in a stacking-like way giving rise to much rougher surfaces. From the profiles and surface roughness values (R_q), it is clear that, by altering the electrolyte on the EHC synthesis process, the surface roughness of the EHC films changes.

Raman spectroscopy was used to investigate structural differences between the different prepared EHC nanomaterials deposited on quartz slides, **Figure 2**. The Raman assignment of the resulting bands in this type of materials was already defined in a previous work [3]. For all the samples, the Raman spectra at the low wavenumber range are dominated by the typical D and G bands. The D mode at ≅ 1350 cm^{-1} is associated to the radial breathing modes of aromatic rings which only become active in the presence of local defects / disorders [5,6], typically induced by the coexistence of sp^3 C atoms [7,8]. The G mode at ≅ 1580 cm^{-1} is attributed to E_{2g} phonon of all sp^2 bonds of carbon atoms, including those in the rings [5,9]. Additionally, a band at ≅ 1200-1250 cm^{-1}, ascribed to C-H chains [10] and a band centred between G and D bands, at ≅ 1500 cm^{-1} (a-C band), are also depicted. The latter is often associated to the presence of an amorphous form of carbon [11,12]. The raw spectra were fitted with the four aforementioned bands to allow comparison of their position, height and

full width of half-maximum (FWHM). The largest FWHM of D and G bands on EHC@glycine, along with a significant contribution of a-C band suggest its lowest structural order compared to the other EHC nanomaterials. EHC@glycine not only seems to be more amorphous, but also appears to contain more species other than just allotropic forms of carbon, as suggested by the relative intensity of the band at ≅ 1200-1250 cm^{-1}.

The presence of small modulated bumps at the high wavenumber region, instead of well-defined second-order Raman peaks, is also consistent with a disorder structure. The fitting procedure allows the detection of three broad bands at ≅ 2740 cm^{-1} (2D band, from a double resonance phenomenon), ≅ 2940 cm^{-1} (D + G mixed mode overlapped with sp^3 C-H stretching modes) and ≅ 3200 cm^{-1} (possibly 2D´ mode overlapped with sp^2 C-H vibration modes) on EHC@phosphate and EHC@citrate, but not on EHC@glycine. The breakdown of the second order spectrum structure of EHC@glycine is also consistent with its higher amorphicity.

EHC prepared in different buffer solutions were also characterized by XPS. C 1s spectra are depicted in **Figure 3** and corresponding data is summarized in **Table 1**.

The peaks fitted in C 1s regions are similar to those described in detail and identified in our previous works [1,2]. The result of the C 1s peak-fitting is shown in **Figure 3a**. The main peaks centred around 285 eV include peaks corresponding to sp^2 carbon atoms (284.4-284.7 eV) and to sp^3 carbon (285 eV) (**Table 1**). From (roughly) 285 to 287 eV, one can find carbon atoms singly bound to oxygen (286.7 eV) and, particularly in the material prepared in the glycine solution, carbon singly bound to nitrogen (285.6-286.4 eV). Also in this region, other features like carbon atoms suffering inductive effects from other carbon atoms (***C***-C<), can be superimposed [1,13].The B.E. of 288.0 eV is typical of carbon in carbonyl groups or O-***C***-O, but the presence of carboxylate groups cannot be discarded given the reactional media in use. EHC prepared in citrate also presents a peak centred at 289.4 eV, assigned to carboxyl groups. This peak can also be present in the other samples, but included in the peaks centred above 290.0 eV, which are mainly from carbonate groups.

In addition to carbon and oxygen (which includes oxygen from inorganic ionic species (≤ 532.0 eV) and oxygen from carbonaceous species as described above (533.0 eV)), others elements were also detected, namely, nitrogen, sodium and chlorine (**Table 1**). Regarding nitrogen, carbon-nitrogen bond formation was detected before by XPS and ATR-FTIR in EHC nanomaterials [1]. Its origin was attributed to N_2 present in the air and/or in aqueous media during graphite electrodes polarization. This anomalous phenomenon was interpreted as the result of the very high electric field established between the anodic and cathodic compartment of the electrochemical cell (20 V/cm), leading to the formation of very reactive carbon-based species (most probably radical species), which would be would be able to react with the N_2 gas present in the aqueous medium or/and in the atmosphere. In the present work the amount of nitrogen detected in EHC@glycine is 3 times larger than in other samples, indicative that the nitrogen-containing electrolyte may itself contribute to the incorporation of nitrogen in the carbon-based material, reinforcing the hypothesis that formation of highly reactive carbon-based species may occur along the EHC generation. This behaviour is still under investigation. It is not excluded the hypothesis that the grade of amorphicity detected by Raman on EHC@glycine film may be related to its high content on nitrogen.

N 1s was fitted with a single peak centered at 400.1 eV, **Figure 3b**, which is indicative that the same N-functional group must have been formed in the three different EHC materials. However, it is not excluded the hypothesis that other peaks may be included. Actually, it is very difficult to distinguish and quantify accurately the N-groups in carbon´s framework (pyridinic-N, pyrrolic-N, graphitic-N or quaternary-N), which is probably the main reason for the controversial results and conclusions found in the literature about the adequate N-active sites for the ORR [14]. Regarding the O/C atomic ratio, it is approximately three times larger in EHC@phosphate than in the other samples (in EHC@glycine and EHC@citrate, O/C is, within the experimental error, the same), which is indicative of the higher oxidation state of EHC@phosphate.

In EHC@phosphate and EHC@citrate, the presence of the ionic species Na^+, Cl^- or Ca^{2+} is not fully counterbalanced by the carbonaceous charged species identified above (namely, COO^- and CO_3^{2-}), as shown by the charge balance > 0 (Table 1). As postulated before [1, 2], negative charges in π delocalized systems may be present to neutralize the cations detected. Another hypothesis is the formation of very strong dipoles on the surface of the electrode material, leading to long-range electrostatic attraction of positive charge species. Such dipolar effect, caused by the polarization of π electrons, has been recently demonstrated by Martin et al. for polycyclic aromatic hydrocarbons curved by pentagon incorporation [15]. In EHC@glycine, the positive charge is, apparently and within the experimental error, balanced by the identified anions (Total charge ≈ 0).

In brief, the characterization of EHC materials by AFM, Raman and XPS allowed us to conclude that the buffer electrolyte affects the surface chemical state (highest O/C in EHC@phosphate), the disorder degree in the hexagonal sp^2 carbon network (highest disorder degree in EHC@glycine), oxygen functional groups (carboxyl groups are only displayed on EHC@citrate) and surface roughness (highest in EHC@phosphate and lowest in EHC@glycine). Although evidence for the incorporation of nitrogen was given in three different EHC materials, the same type of N-functional group seems to be formed.

3.2. Electrochemical behaviour of EHC films

Cyclic voltammetry was used to study the electrode response of the different prepared EHC nanomaterials in the presence of an outer-sphere and inner-sphere redox couple, $[Fe(CN)_6]^{3-/4-}$ and $[Ru(NH_3)_6]^{3+/2+}$, respectively, in a 1 M KCl solution, **Figure 4**.

It is evident that the electrode responses to $[Ru(NH_3)_6]^{3+/2+}$ probe are very similar, showing the same anodic to cathodic peak-to-peak separations (ΔE_p) and therefore, comparable electronic properties (density of the electronic states near the formal potential). The apparent heterogeneous electron-transfer rate constant (k^0_{ap}), calculated by Nicholson's method, was

found to be 1.46 x 10^{-3} cm s^{-1}. Curiously, this value differs considerably from k^0_{ap} found on EHC films that display a low content of nitrogen (0.065 cm s^{-1}) [3] and on reduced graphene films (0.18 cm s^{-1}) [16], but it is in the same order on nitrogen containing amorphous carbon this films (5 x 10^{-3} cm s^{-1})[17].

By investigating the dependence of j_p on the square root of the scan rate (inset Fig 4a) using the Randles-Sevcik equation, the electroactive surface areas were evaluated. It was found 0.134, 0.090 and 0.085 cm^2 to EHC@phosphate, EHC@citrate and EHC@glycine films, respectively. Although these values follow the trend of R_q data obtained from AFM images, a greater difference between the electrochemical surface area of EHC@citrate and EHC@glycine films was expected. At this point we do not have an explanation for this behaviour.

In contrast, for the $[Fe(CN)_6]^{3-/4}$ redox couple, large differences on the ΔEp are observed, indicative of significant differences on the interaction of this anion with the surface of the EHC nanomaterial. Specifically, these chemical interactions could involve electrostatic or site-blocking effects. Commonly, a decrease of ΔEp with the increase of the C/O ratio of the material is found [18,19]. However, an opposite behaviour is discerned in this work. We suppose that the highest ΔEp, observed on EHC@citrate, may reflect to a certain extent the content of surface oxygen functionalities that are ionizable, like carboxyl groups, which lead to the electronic repulsion of $[Fe(CN)_6]^{3-/4-}$ and consequently, to more sluggish electrode kinetics. Actually, this carbon-oxygen functionality was explicitly detected by XPS on EHC@citrate, but not on the other two EHC nanomaterials. k^0_{ap}, calculated by Nicholson's method, was found to be 5.48 x 10^{-4} cm s^{-1}, 1.12 x 10^{-4} cm s^{-1} and 3.43 x 10^{-4} cm s^{-1} for EHC@phosphate, EHC@citrate and EHC@glycine films, respectively. Hence, in $[Fe(CN)_6]^{3-/4-}$ solution, the EHC@phosphate shows superior ability for the heterogeneous electron transfer.

3.3 Electrocatalytic reduction of H_2O_2

Figure 5 shows the typical cyclic voltammograms (1^{st} and 15^{th} scan – solid and dashed line, respectively) of the different EHC nanomaterials cast on a glassy carbon electrode in a 0.1 M phosphate buffer solution (pH= 7.0) containing 6.2 mM H_2O_2. In comparison with the bare glassy carbon electrode, the current reduction of H_2O_2 on the three EHC films is markedly enhanced and the reduction potential onset is shifted positively, pointing for an electrocatalytic electrode reaction. However, compared to other carbon-based materials, like electrochemically reduced graphene oxide (E_p at -0.25 V *vs* Ag/AgCl) [20] or nitrogen doped graphene (E_p at -0.40 V *vs* Ag/AgCl) [21] it requires a larger overpotential. Nevertheless, our results reveal that the magnitude of the required overpotential and current magnitude is dependent on the electrolyte used to synthesise the EHC nanomaterial. The first scan of the cyclic voltammograms shows that EHC@citrate and EHC@phosphate display a similar catalytic activity towards H_2O_2, whereas EHC@glycine is significantly less catalytic. However, along repetitive cycles this behaviour is meaningfully changed: the potential onset for the H_2O_2 reduction on EHC@citrate shifts drastically to more positive potentials (corresponding to a 300 mV overpotential decrease), while an opposite effect is observed on EHC@phosphate. Regarding EHC@glycine film, its activity slightly enhances along successive cycles. These results suggest that species formed upon the hydrogen peroxide electrochemical reduction on EHC films may play an inhibiting or catalytic role in the overall reduction reaction, strongly depending on the electrolyte that was used on the EHC synthesis.

Remarkably differences were also found on investigating by linear voltammetry the reduction current magnitude dependence on the H_2O_2 concentration (**Figure 6**). In these experiments successive additions of H_2O_2, intercalated with a resting time at open circuit potential of approximately 90 s, were undertaken. The plot of the current data as a function of the H_2O_2 concentration at a constant potential (e.g. -1.2 V), **Figure 6b**, shows that a good linear correlation is found on EHC@citrate over the concentration understudy (with a detection limit of 0.184 mM and a sensitivity of 0.167 mA cm^{-2} mM^{-1}), whereas a non-linear relationship is

found on EHC@glycine and a negative deviation from linearity is exhibited by EHC@phosphate at concentrations as low as 3.0 mM. These results show that among the aforementioned EHC nanomaterials, EHC@citrate is the most suitable for analytical purposes.

It is important to remark that the meaningful differences between EHC@phosphate and EHC@citrate cannot be imputed to the amount of nitrogen contained in the nanomaterial, since both exhibit exactly the same amount.

By comparing the current response of the EHC films obtained directly in a 6.0 mM H_2O_2 solution (Figure 5), with those acquired in the same concentration solution but after successive small additions of H_2O_2, (Figure 6), it is noted that the current recorded upon the successive increments of H_2O_2 is ≅ 5-fold lower on EHC@phosphate (e.g. decreases from -0.97 to -0.21 mA cm^{-2} at -1.20 V) and ≅ 1.4-folder higher on EHC@glycine (e.g increases from -0.25 to -0.34 mA cm^{-2} at -1.20 V). On EHC@citrate no changes were observed. The results obtained on EHC@phosphate and EHC@glycine resemble the behaviour observed upon successive scans (Figure 4), suggesting the formation of surface species that have, respectively, an inhibition and catalytic effect on the hydrogen peroxide reduction. In order to evaluate whether the formation of such species occurs in a time dependent reaction, two different essays were undertaken. First, it was evaluated the effect of holding the electrode in the peroxide solution (from 0 to 1 hour) at open circuit potential before the first voltammogram was recorded. It was observed that this resting time had no effect. Another experiment was carried out by recording, immediately after the first voltammetric scan, voltammograms with increasing waiting time of the electrode at open circuit potential in the peroxide solution. Remarkable differences between the three electrode materials were obtained, **Figure 7**. Unexpectedly, a significant increase of the cathodic current and a meaningful shift of the potential reduction onset is shown on EHC@glycine. For example, at -0.1 mA cm^{-2}, a remarkable 500 mV decrease on the H_2O_2 reduction overpotential after one resting hour in the peroxide solution is observed. On EHC@citrate just a moderate increase is detected, whereas no time dependent

evolution seems to occur on the voltammograms recorded on EHC@phosphate. Importantly, no blocking-like effect is discerned on this electrode material, contrasting to what was observed upon successive voltammetric cycles and successive additions of H_2O_2. These results suggest that the blocking-like effect showed on EHC@phosphate may result from surface species that may be produced along the H_2O_2 electrochemical reduction, diminishing the available EHC surface sites for further reduction of H_2O_2. However, if a long resting time is given between voltammetric essays, these species may desorb (or further react), resulting new surface sites available for the ongoing electrochemical reduction of peroxide.

The overall results obtained with EHC@glycine point out for the formation of chemical species which are themselves the catalyst of the peroxide electrochemical reduction reaction, resembling an autocatalytic-type reaction. Actually, the time dependent effect is indicative that such catalytic species would not be the electrochemical reduction product itself, but it would be formed, in a time dependent chemical reaction triggered by species produced by the H_2O_2 electrochemical reduction. Most probably, this chemical reaction would involve adsorbed species on the EHC film. To confirm our assumption, another experiment was performed by rotating the electrode immediately after the reduction scan. It was shown that in such conditions there was no catalytic effect, even if keeping the electrode in solution for long periods. This result confirms the involvement of adsorbed species on the chemical reaction that are responsible for the formation of the catalytic species. The surface species could be provided by the H_2O_2 electrochemical reduction reaction (species A) or/and the product of the chemical reaction that follows immediately the electrochemical reaction (species P), **Figure 11**. The proposed mechanism outlined in equation (1) to (4) provides also a comprehensive interpretation of the results obtained on EHC@citrate. Actually, admitting that the species that would participate on chemical reaction (2) are very weakly adsorbed, a catalytic effect would be only expectable if uninterrupted voltammetric essays are performed. If long resting times at open circuit potential are given between the voltammetric scans, species A and/or P would

desorb and diffuse away from the surface (equations 3 and 4). Consequently, their catalytic effect would no longer be observed. Hence the main differences between EHC@citrate and EHC@glycine may rely on the different adsorption strength of A and/or P on the surface electrode material.

At this point it is not clear if the mechanism that occurs on EHC@phosphate involves a completely different intermediate, or very different rate reactions. A literature survey reveals that an autocatalytic mechanism was already proposed for the reduction of H_2O_2, but in silver electrodes in acid medium [22]. In that case, it was suggested that the catalytic species is adsorbed OH, formed as an intermediate in the H_2O_2 reduction reaction, which in turn, allows the reduction of peroxide to proceed faster.

Although further studies would be required to identify the intermediate species formed on EHC materials, the results exhibited by EHC@glycine are very interesting and may be explored in the future as a mean to increase the reactivity of hydrogen peroxide. In a different framework, the results shown by the EHC@phosphate may have an important impact in the design of sensors that usually require a permselective membrane to avoid hydrogen peroxide interference.

3.4 Electrocatalytic reduction of O_2

The EHC films, cast on a glassy carbon disk electrode, were placed in a Ar-saturated 0.1 M phosphate buffer solution, and their potential was scanned between the open circuit potential ($\cong$ 0.05 V) and -1.20 V, until a steady-state voltammogram was reached. Then, the solution was saturated with O_2 and the polarizations curves were recorded at 20 mVs^{-1} at successive higher rotation rates, from 0 to 2100 rpm.

For an effective comparison of the potential onset, both the linear scanning voltammograms (LSV) measured at zero rotation rate (corrected for background current) and 1600 rpm were

recorded for the different EHC nanomaterials in the O_2-saturated solution, **Figure 8a,8b**. The first interesting feature to note, is the large overpotential increase on the reduction potential onset of EHC@phosphate upon the electrode rotation (≅ 250 mV), whereas no substantial difference is observed on EHC@glycine and EHC@citrate electrodes. The reason for this phenomenon is not clear but the assumption that phosphate ions are adsorbed on the EHC@phosphate surface is not discarded (and consequently, their role on the inhibition of the H_2O_2 reduction reaction). Although the interaction of phosphate ions with EHC films has never been investigated, the interaction of phosphate with others carbon-based materials is known [23–25]. Apart from this singularity, it is concluded from the potentials onset that EHC@citrate displays the highest catalytic activity (**Table 2**). The obtained value (-0.21 V *vs* Ag/AgCl or 0.41 V *vs* RHE) are comparable to that of state-of-art nitrogen-doped carbon-based materials [26–29].

A second feature of interest arises on comparing the current densities on the different EHC films within the -0.60 to -1.20 V potential range in non-rotating essays. It is shown that the current magnitude follows the same trend depicted in solutions with H_2O_2 (Figure 5), suggestive that peroxide is an intermediate species on the oxygen reduction mechanism.

Linear scanning voltammograms at increasing rotations rates are presented in **Figure 9**. It is shown that a flat plateau current is not achieved, even at low rotation rates. The inclination of the current plateaux leads to a non-reliable estimation of the true limiting current. The presence of an inclined plateau has been found on electrodes with a thin porous coating and slow kinetics, and has been interpreted as the reduction of O_2 at high overpotentials is not only limited on the outer part of the porous electrode, but also within the pores of the catalyst, where the depth of O_2 penetration changes with potential [30,31] .

The mass activity was also calculated (current normalized to the mass of catalyst) to compare the intrinsic activity of the different prepared EHC nanomaterials (Table 2). The mass activity was determined by extracting the mass transport corrected current at -0.35 V, which was

chosen from the kinetically controlled potential region, as revealed by the rotating disk electrode essays. The obtained values show unequivocally that EHC@citrate exhibits a much higher catalytic activity to the ORR than the EHC prepared in phosphate or glycine buffer solutions. This conclusion is also supported by the mass transfer Tafel slope data in the low overpotential region, wherein EHC@citrate exhibits the lowest value (115 mV dec^{-1}). Even so, the obtained data is rather high compared to Pt/C (≅ 60 mV dec^{-1}) [32]. The uncommon high Tafel slope obtained on EHC@phosphate (239 mV dec^{-1}), may reflect the blocking-like effect that occurs throughout the peroxide reduction reaction, as demonstrated above.

In summary, the potential onset data, Tafel slope and mass activity values, allow to conclude that the catalytic activity of EHC nanomaterials towards the ORR is strongly dependent on the nature of the electrolyte used on the electrochemical synthesis. The hydrophilic carbon nanomaterial electrogenerated in citrate displays unequivocally the highest activity, whereas a lower catalytic activity is found if phosphate or glycine is used. The non-correlation between the nitrogen content on the EHC materials and their catalytic activity are indicative that the incorporation of nitrogen in the carbon framework does not create favourable surface sites for the ORR.

Using the data presented in **Figure 9a**, Koutecky-Levich plots (I^{-1} vs $\omega^{-1/2}$) were constructed for -0.8 to -1.2 V potential range, **Figure 9b**, to predict the number of electrons transferred. Accordingly, Koutecky-Levich equation is given by

$$\frac{1}{i} = \frac{1}{i_k} + \frac{1}{i_L} = \frac{1}{i_k} + \frac{1}{0.62\, n\, F\, A\, D_o^{2/3} \nu^{-1/6}\, C_{O2}}$$

where *n* is the number of electrons transferred per oxygen molecule, *F* is faraday´s constant, *A* is the geometric surface area (predicted from data obtained with $Ru(NH_3)_6^{3+/2+}$ redox probe), D_0 is the diffusion coefficient of oxygen (1.9 x10^{-5} cm^2 s^{-1}), ν is the kinematic viscosity of the electrolyte (1.0x10^{-2} cm^2 s^{-1}), C_0 is the bulk concentration of oxygen in the solution (1.2x10^{-6} mol cm^{-3}) and ω is the rotation rate of the RDE (in rad s^{-1}).

The linear responses are consistent with a reaction order of one with respect to O_2. However, the nonzero intercept for the limiting currents support the assumption that there is not a complete diffusion control, i.e. the kinetic control of the reaction is not negligible at the aforementioned potential range. It is possible, as stated before, that the reaction does not occur solely on the top of the surface, but also within the pores catalyst, resulting an uncertainty in the real surface area accessible to O_2. Hence, the slope of the Koutechy-Levich plot was used to provide a rough estimation of the number of electrons transferred within the potential range between -0.80 and -1.20 V, **Figure 10**. Accordingly, on EHC@phosphate, the number of electrons is approximately one, independent of the electrode potential, whereas on EHC@citrate a two-electron pathway is depicted at -0.80 V, shifting to 2.7 at -1.20 V. The number of electrons transferred on EHC@glycine shows that this material catalyses both the 2e and 4e pathways, within the -0.80 to -1.20 V potential range, although the 2e pathway is the most dominant one.

In summary, it was concluded that the most catalytic material for the ORR is EHC@citrate, although EHC@glycine shows the highest conversion of O_2 to H_2O, in agreement with the electrochemical behaviour observed in the hydrogen peroxide solution. The overall results show that there is no correlation between the nitrogen content (admitting one single type of N-functional group) and the electrocatalytic activity towards the O_2 and H_2O_2 reduction reactions. Hence, other factors rather the incorporation of nitrogen in the carbon´s framework, must be responsible for the catalytic activity. The analysis of a 3D plot between representative electrocatalytic descriptors for the ORR (number of electrons transferred and mass activity) and main surface characterization descriptors per EHC material may highlight some important relationships. Accordingly, Figure 12 shows that a high surface roughness, or high O/C ratio, does not promote the ORR activity of EHC materials. On the contrary, a smooth surface seems to be required for an efficient conversion of oxygen to water. In addition, it is also shown that the nature of oxygen functional groups has an important effect on the ORR.

For instance, the mass activity is rather high on EHC containing an important amount of carboxyl groups whereas an opposite effect is observed on EHC having a high content of carbonyl groups. It is also revealed that a high content of oxygen functional groups containing oxygen single bonded to carbon (ethers and/or alcohols) and a high disorder degree in sp^2 carbon network (represented by the FWHM data) have an important effect on the number of electrons transferred. Actually, a strong correlation between C-O content and the number of electrons transferred is depicted. Hence, we may conclude that an interplay between surface defects and oxygen functional groups effects may be responsible for the catalytic activity of EHC materials for the ORR.

4. Conclusions

It was concluded that despite the buffer electrolyte does not affect the electronic conductivity of the EHC materials (which was appraised by cyclic voltammetry in $Ru(NH_3)_6^{3+}$ solution), it affects the surface chemical state (O/C content is 3 times larger in EHC@phosphate than in EHC@citrate or EHC@glycine), the disorder degree in the hexagonal sp^2 carbon network (EHC@glycine exhibits the highest disorder degree), oxygen functional groups (carboxyl groups are only displayed on EHC@citrate) and surface roughness (EHC@glycine shows the smoothest surface). It was also concluded that the most catalytic material for the ORR is EHC@citrate, but the highest conversion of O_2 to H_2O occurs on EHC@glycine ($n \cong 2.7$ to 3.0). This behaviour is in line with the electrochemical behaviour observed in H_2O_2. Accordingly, a very singular behaviour in the electrochemical reduction of hydrogen peroxide was found on EHC@glycine, qualitatively interpret as an autocatalytic reaction. In contrast, a blocking-like effect was observed on EHC@phosphate. Although evidence for the N-C bond was found on all EHC materials, the overall results are indicative that the ORR and H_2O_2 reduction do not occur at the N-containing surface sites of the EHC material. In light of the undertaken physicochemical characterization, it was concluded that the nature of oxygen functional groups has an

important effect on the ORR: C-O and COOH groups promote the catalytic activity, whereas C=O groups have an opposite effect. It was concluded that an interplay between surface defects and oxygen functional groups effects may be responsible for the catalytic activity of EHC materials for the ORR.

This work clearly demonstrates that it is possible to modulate the properties of EHC nanomaterials by choosing a suitable buffer electrolyte, but further efforts will be required to understand the mechanism responsible for the buffer electrolyte effect on the generation of the EHC nanomaterial and for a better elucidation of the nature of the surface catalytic sites.

Acknowledgements

This work was supported by Fundação para a Ciência e Tecnologia (FCT), FEDER under programme PT2020 through projects UID/QUI/00616/2013, UID/MULTI/00612/2013, UID/NAN/50024/2013 and project "UniRCell" with the reference POCI-01-0145-FEDER-016422. A. S. V. acknowledges FCT for projects IF/00808/2013/CP1159/CT0003 and A. M. Ferraria acknowledges FCT for Grant SFRH/BPD/108338/2015. We also thank Prof. João Coutinho (UTAD) for TOC analysis.

References

[1] A.D. Veloso, A.M. Botelho do Rego, A.M. Ferraria, L.F.V. Ferreira, D.P. Ferreira, P.B. Tavares, R. Videira, A.S. Viana, M.C. Oliveira, One-Step Cathodic and Anodic Synthesis of Hydrophilic Carbon Nanomaterials, ChemElectroChem. 4 (2017) 2693–2702. doi:10.1002/celc.201700386.

[2] M.C. Oliveira, A.S. Viana, M. Botelho, A.M. Ferraria, P.B. Tavares, A.D. Veloso, R.A. Videira, Dual Behaviour of Amorphous Carbon Released Electrochemically from Graphite, ChemistrySelect. 1 (2016) 4126–4130. doi:10.1002/slct.201600965.

[3] R.S. Vieira, A.J.S. Fernandes, M.C. Oliveira, Electrochemical behaviour of electrogenerated hydrophilic carbon nanomaterials, Electrochimica Acta. 260 (2018) 338–347. doi:10.1016/j.electacta.2017.10.197.

[4] H. Wei, E. Wang, Nanomaterials with enzyme-like characteristics (nanozymes): next-generation artificial enzymes, Chemical Society Reviews. 42 (2013) 6060. doi:10.1039/c3cs35486e.

[5] A.C. Ferrari, J. Robertson, Interpretation of Raman spectra of disordered and amorphous carbon, 61 (2000) 95–107.

[6] A.C. Ferrari, Determination of bonding in diamond-like carbon by Raman spectroscopy, 11 (2002) 1053–1061.

[7] D. Beeman, J. Silverman, R. Lynds, M.R. Anderson, Modeling studies of amorphous carbon, Physical Review B. 30 (1984) 870–875. doi:10.1103/PhysRevB.30.870.

[8] S.-H. Hong, J. Winter, Micro-Raman spectroscopy on a-C:H nanoparticles, Journal of Applied Physics. 98 (2005) 124304. doi:10.1063/1.2142078.

[9] A.C. Ferrari, Raman spectroscopy of graphene and graphite: Disorder, electron-phonon coupling, doping and nonadiabatic effects, Solid State Communications. 143 (2007) 47–57. doi:10.1016/j.ssc.2007.03.052.

[10] A.J.S. Fernandes, M.A. Neto, F.A. Almeida, R.F. Silva, F.M. Costa, Nano- and micro-crystalline diamond growth by MPCVD in extremely poor hydrogen uniform plasmas, 16 (2007) 757–761. doi:10.1016/j.diamond.2006.12.029.

[11] H.M.I. Jaim, D.P. Cole, L.G. Salamanca-riba, Characterization of carbon nanostructures in Al and Ag covetic alloys, Carbon. 111 (2016) 309–321. doi:10.1016/j.carbon.2016.10.007.

[12] S.A. Chernyak, A.S. Ivanov, K.I. Maslakov, A. V Egorov, Z. Shen, S. Savilov, V. V Lunin, Oxidation, defunctionalization and catalyst life cycle of carbon nanotubes: a Raman spectroscopy view†, Physical Chemistry Chemical Physics. 19 (2017) 2276–2285. doi:10.1039/C6CP04657F.

[13] D. Beamson, G. & Briggs, High resolution XPS of organic polymers. The Scienta ESCA300 Database, John Wiley, 1992.

[14] D. Xiong, X. Li, L. Fan, Z. Bai, Three-Dimensional Heteroatom-Doped Nanocarbon for Metal-Free Oxygen Reduction Electrocatalysis: A Review, Catalysts. 8 (2018) 301. doi:10.3390/catal8080301.

[15] J.W. Martin, R.I. Slavchov, K.Y. Edward, J. Akroyd, S. Mosbach, M. Kraft, The Polarization of Polycyclic Aromatic Hydrocarbons Curved by Pentagon Incorporation : The Role of the Flexoelectric Dipole The Polarization of Polycyclic Aromatic Hydrocarbons Curved by Pentagon Incorporation : The Role of the Flexoelectric Dipole, (2017). doi:10.1021/acs.jpcc.7b09044.

[16] L. Tang, Y. Wang, Y. Li, H. Feng, J. Lu, J. Li, Preparation, structure, and electrochemical properties of reduced graphene sheet films, Advanced Functional Materials. 19 (2009) 2782–2789. doi:10.1002/adfm.200900377.

[17] X. Yang, L. Haubold, G. Devivo, G.M. Swain, Electroanalytical Performance of Nitrogen-Containing Tetrahedral Amorphous Carbon Thin-Film Electrodes, (2012).

[18] S.M. Tan, A. Ambrosi, C.K. Chua, M. Pumera, Electron transfer properties of chemically reduced graphene materials with di ff erent oxygen contents, (2014) 10668–10675. doi:10.1039/c4ta01034e.

[19] M.C. Granger, G.M. Swain, The Influence of Surface Interactions on the Reversibility of Ferri / Ferrocyanide at Boron-Doped Diamond Thin-Film Electrodes, 146 (1999) 4551–4558.

[20] S. Mutyala, J. Mathiyarasu, A reagentless non-enzymatic hydrogen peroxide sensor presented using electrochemically reduced graphene oxide modi fi ed glassy carbon electrode, 69 (2016) 398–406. doi:10.1016/j.msec.2016.06.069.

[21] L. Magerusan, F. Pogacean, C. Socaci, M. Coros, M. Rosu, S. Pruneanu, Electrochimica Acta Charge transfer-resistance in nitrogen-doped / undoped graphene : Its in fl uence on the electro-catalytic reduction of H 2 O 2, Electrochimica Acta. 220 (2016) 664–671. doi:10.1016/j.electacta.2016.10.139.

[22] K. Doblhofer, G. Flätgen, S. Horswell, B. Pettinger, S. Wasle, K.G. Weil, Autocatalysis by the intermediate surface hydroxide formed during hydrogen peroxide reduction on silver electrodes, Surface Science. 603 (2009) 1900–1903. doi:10.1016/j.susc.2008.11.047.

[23] P. Kumar, S. Sudha, S. Chand, V.C. Srivastava, Phosphate Removal from Aqueous Solution Using Coir-Pith Activated Carbon Phosphate Removal from Aqueous Solution Using Coir-Pith Activated Carbon, 6395 (2010). doi:10.1080/01496395.2010.485604.

[24] G.G. Jayson, T.A. Lawless, D. Fairhurst, The Adsorption of Organic and Inorganic Phosphates onto a New Activated Carbon Adsorbent, 86 (1982).

[25] P.A. Trazzi, J.J. Leahy, M.H.B. Hayes, W. Kwapinski, Journal of Environmental Chemical Engineering Adsorption and desorption of phosphate on biochars, 4 (2016) 37–46.

[26] X. Zhang, Y. Chen, J. Wang, Q. Zhong, Nitrogen and fluorine dual-doped carbon black as an efficient cathode catalyst for oxygen reduction reaction in neutral medium, (2016) 696–702. doi:10.1002/slct.201600144.

[27] L. Sun, Y. Luo, M. Li, G. Hu, Y. Xu, T. Tang, J. Wen, X. Li, L. Wang, Journal of Colloid and Interface Science Role of Pyridinic-N for Nitrogen-doped graphene quantum dots in oxygen reaction reduction, Journal of Colloid And Interface Science. 508 (2017) 154–158. doi:10.1016/j.jcis.2017.08.047.

[28] G. Tao, L. Zhang, L. Chen, X. Cui, Z. Hua, M. Wang, J. Wang, Y. Chen, J. Shi, N-doped hierarchically macro / mesoporous carbon with excellent electrocatalytic activity and durability for oxygen reduction reaction, Carbon. 86 (2015) 108–117. doi:10.1016/j.carbon.2014.12.102.

[29] D. Guo, R. Shibuya, C. Akiba, S. Saji, T. Kondo, J. Nakamura, Active sites of nitrogen-doped carbon materials for oxygen reduction reaction clarified using model catalysts, 351 (2016) 361–365.

[30] S. Gupta, R.F. Savinell, Heat-treated iron (III) tetramethoxyphenyl porphyrin chloride supported on high-area carbon as an electrocatalyst for oxygen reduction Part II . Kinetics of oxygen reduction, 462 (1999) 63–72.

[31] P.H. Matter, L. Zhang, U.S. Ozkan, The role of nanostructure in nitrogen-containing carbon catalysts for the oxygen reduction reaction, 239 (2006) 83–96. doi:10.1016/j.jcat.2006.01.022.

[32] S.L. Gojkovi, S.K. Zecevic, R.F. Savinell, 02 Reduction on an Ink-Type Rotating Disk Electrode Using Pt Supported on High-Area Carbons, 145 (1998).

Captions

Figure 1- AFM images, corresponding height profiles and roughness values (Rq), of EHC@citrate, EHC@phosphate and EHC@glycine.

Figure 2-Raman spectra of EHC@phosphate, EHC@citrate and EHC@glycine materials deposited on quartz slide and the corresponding peak positions, FWHM, $I_{a\text{-}C}/I_G$ and I_D/I_G of D, G and a-C bands.

Figure 3- a) C 1s spectra of EHC@citrate, EHC@glycine and EHC@phosphate materials. See text for assignment details. b) N 1s spectra of EHC@citrate, EHC@glycine and EHC@phosphate materials.

Figure 4 - Cyclic voltammograms of GC and GC modified electrodes (EHC@citrate, EHC@glycine and EHC@phosphate) in (a) 1 mM $Ru(NH_3)_6Cl_3$ + 0.1 M KCl and b) 1 mM $K_4Fe(CN)_6$ + 0.1 M KCl solutions. ν = 20 mV s^{-1}. In a) it is included the plot of I_p vs $\nu^{0.5}$.

Figure 5 - Cyclic voltammograms of GC and GC modified electrodes (EHC@citrate, EHC@glycine and EHC@phosphate) in 0.1 M PB solution containing 6.2 mM H_2O_2. 1st and 15th scans (full and dashed lines, respectively); ν = 50 mV s^{-1}.

Figure 6 – a) Cyclic voltammograms of EHC@citrate, EHC@glycine and EHC@phosphate in 0.1 M PB solution containing different H_2O_2 concentrations and b) corresponding plots of the current density at -1.20 V as a function of the hydrogen peroxide concentration.

Figure 7- Cyclic voltammograms of EHC@citrate, EHC@glycine and EHC@phosphate measured at different waiting time immersion in 0.1 M PB solution containing 6.2 mM H_2O_2. The time immersion was recorded after the first voltammetric cycle was undertaken.

Figure 8- a) - Linear voltammograms (LV) of GC and GC modified electrodes (EHC@citrate, EHC@glycine and EHC@phosphate) in O_2-saturated 0.1 M PB solution at 0 rpm (included LV in Ar-saturated solutions - dashed lines) and b) 1600 rpm. ν = 20 mV s^{-1}.

Figure 9- a) RDE of polarization curves of GC modified electrodes (EHC@citrate, EHC@glycine and EHC@phosphate) in O_2-saturated 0.1 M PB solution with different rotating speeds at a scan rate of 20 mV s^{-1} and b) corresponding Koutechy-Levich plots at different potentials.

Figure 10- Plot of the number of electrons transferred per O_2 molecule as a function of the electrode potential.

Figure 11- Scheme of the reaction mechanism proposal for the reaction of H_2O_2 on the EHC electrodes.

Figure 12- 3D bar plot of electroactivity descriptors for the ORR and main surface characterization descriptors per EHC material. FWHM (D) and FWHM (G) data were normalized to FWHM of EHC@glycine. Electroactivity descriptors for the ORR: number of electrons transferred at -0.80 v and mass activity at -0.35 V.

Table 1 – Binding Energies, B.E. (eV), averages, corresponding dispersion of values, and assignments; atomic concentrations (%) computed from XPS spectra of anodic compartment solutions; charge balances computed considering all possible charges (≠0) (shadowed lines). * Phosphorus was detected in residual amounts (not quantified).

Table 2- Mass activity at -0.35 V (i_k), potential onset (E_{onset}) and Tafel slope (B) of ORR on GC modified electrodes (EHC@citrate, EHC@glycine and EHC@phosphate).

	B.E. (eV)	Atomic Concentrations (%)			Charge	Assignments
		EHC@phos.	EHC@glyc.	EHC@citr.		
C 1s 1	284.6; 285	22.5	38.9	44.9		***C***-H, C-C sp^2 and sp^3
C 1s 2	285.7 ± 0.2	4.5	8.7	9.9		***C***-C<, ***C***-N, ***C***-O
C 1s 3	286.7 ± 0.1		6.8	2.4		
C 1s 4	288.1 ± 0.1	6.9	6.1	4.3	0 or -1	***C***=O, O-***C***-O, and/or ***C***OO^-
C 1s 5	289.4 ± 0.1			1.7		***C***OOH
C 1s 6	290.5 ± 0.2	2.5	0.9	0.8	-2	***C***O_3^{2-}
O 1s	532.3 ± 0.9	43.6	26.6	23.1		Inorganic ionic species and oxygen bound to carbon
N 1s	400.1 ± 0.1	1.6	4.8	1.5		***N***-C, ***N***-C=O
Na 1s	1071.2 ± 0.1	16.8	7.2	11.2	+1	Na^+
P 2p		*			-3	PO_4^{3-}
Cl 2p	199.0 ± 0.5 ($2p_{3/2}$)	1.4		0.3	-1	Cl^-
Ca 2p	348.3 ± 0.1 ($2p_{3/2}$)	0.2			+2	Ca^{2+}
Total Charge		**3.9**	**-0.8**	**5.2**		Obs.: C 1s 4 being mainly ***C***OO^-
O/C		1.20	0.43	0.36		

Table 1

EHC film	j_k(A g^{-1}) at -0.35 V	B (V/dec)	E_{onset} (V *vs* Ag/AgCl) $\omega \neq 0$	E_{onset} (V *vs* Ag/AgCl) $\omega = 0$
EHC@citrate	0.192	115	-0.21	-0.20
EHC@phosphate	0.067	239	-0.30	-0.04
EHC@glycine	0.043	143	-0.30	-0.22

Table 2

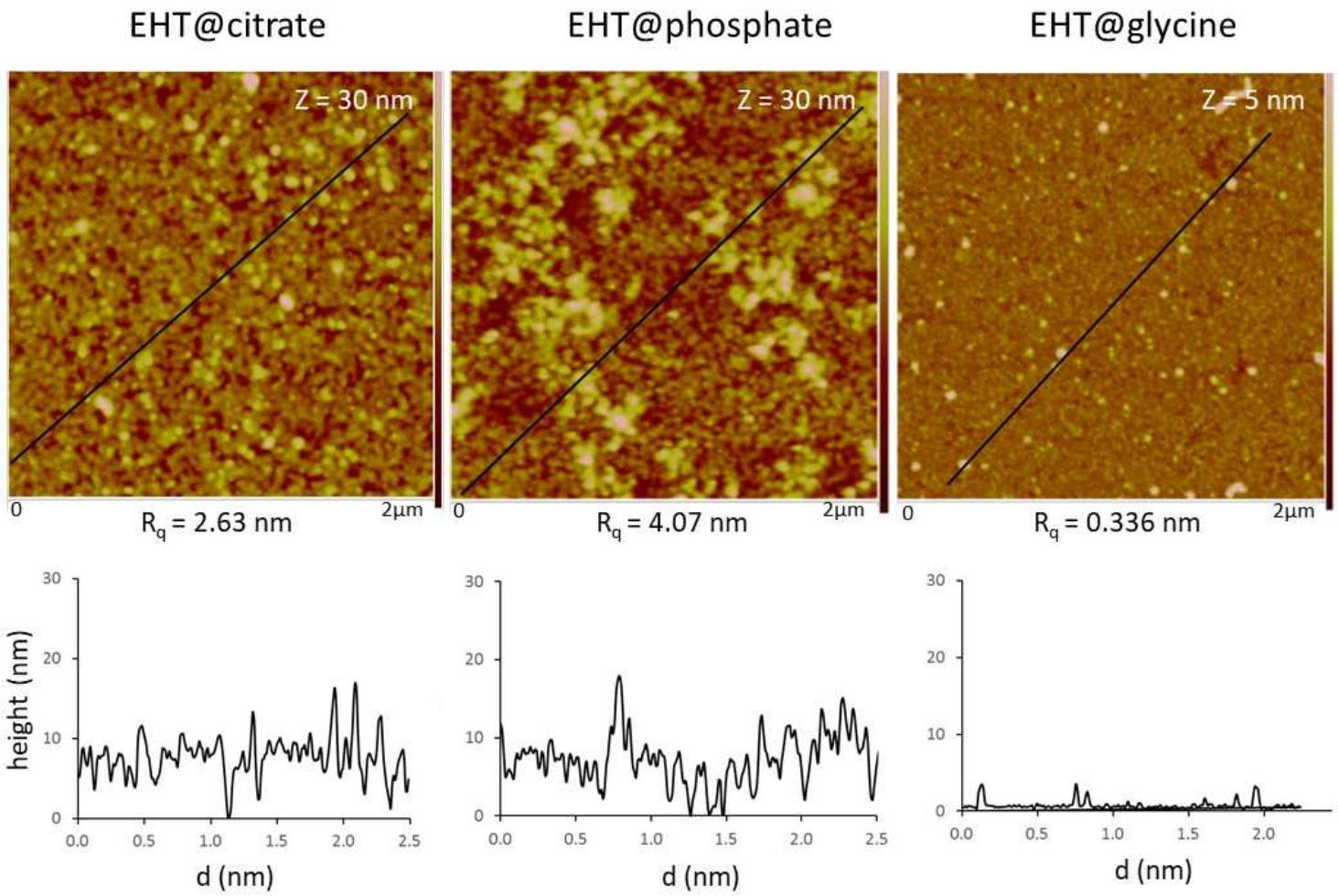
EHT@citrate
EHT@phosphate
EHT@glycine
Z = 30 nm
Z = 30 nm
Z = 5 nm
0
2µm
R_q = 2.63 nm
0
2µm
R_q = 4.07 nm
0
2µm
R_q = 0.336 nm
height (nm)
d (nm)
d (nm)
d (nm)

Figure 1

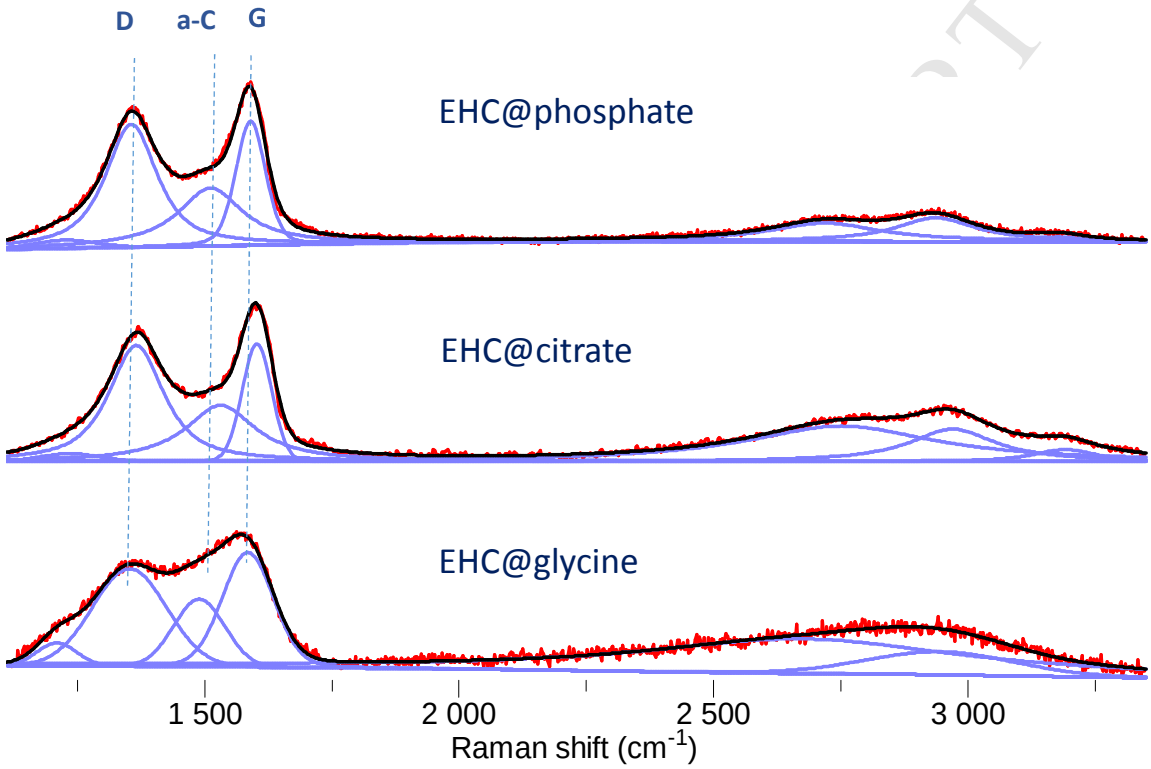

Sample	D		G		a-C		I_{a-C}/I_G	I_D/I_G
	Peak position (cm^{-1})	FWHM (cm^{-1})	Peak position (cm^{-1})	FWHM (cm^{-1})	Peak position (cm^{-1})	FWHM (cm^{-1})		
EHC@citr.	1364.5	128	1601.8	68.4	1530.0	167	0.48	0.99
EHC@phosp.	1356.5	123	1592.0	59.7	1537.2	158	0.69	1.22
EHC@glyc.	1349.9	186	1583.0	119	1485.0	120	0.55	0.95

Figure 2

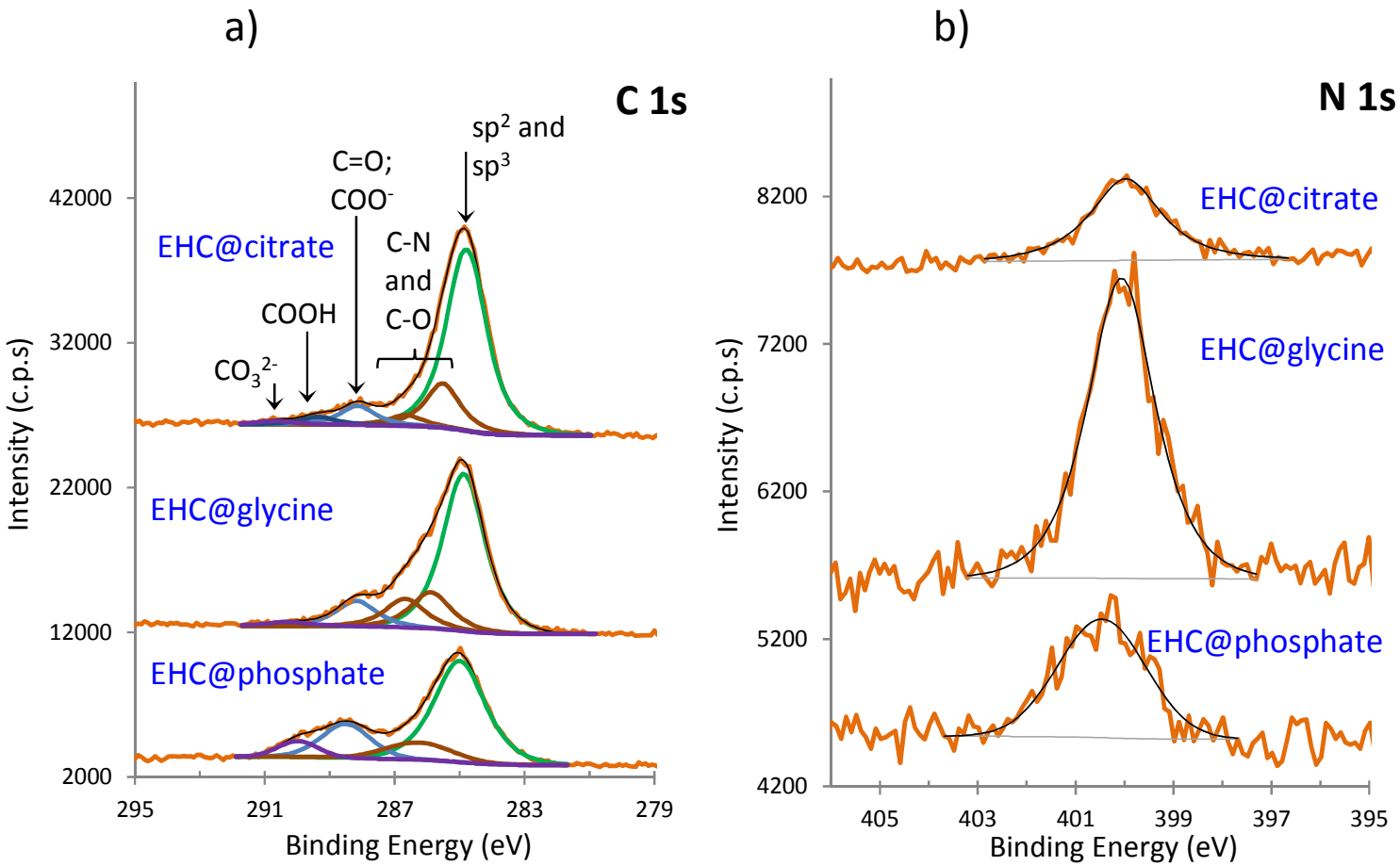
a)
C 1s
sp2 and
sp3
C=O;
COO-
C-N
and
C-O
COOH
CO3 2-
EHC@citrate
EHC@glycine
EHC@phosphate
Intensity (c.p.s)
42000
32000
22000
12000
2000
295
291
287
283
279
Binding Energy (eV)
b)
N 1s
EHC@citrate
EHC@glycine
EHC@phosphate
Intensity (c.p.s)
8200
7200
6200
5200
4200
405
403
401
399
397
395
Binding Energy (eV)

Figure 3

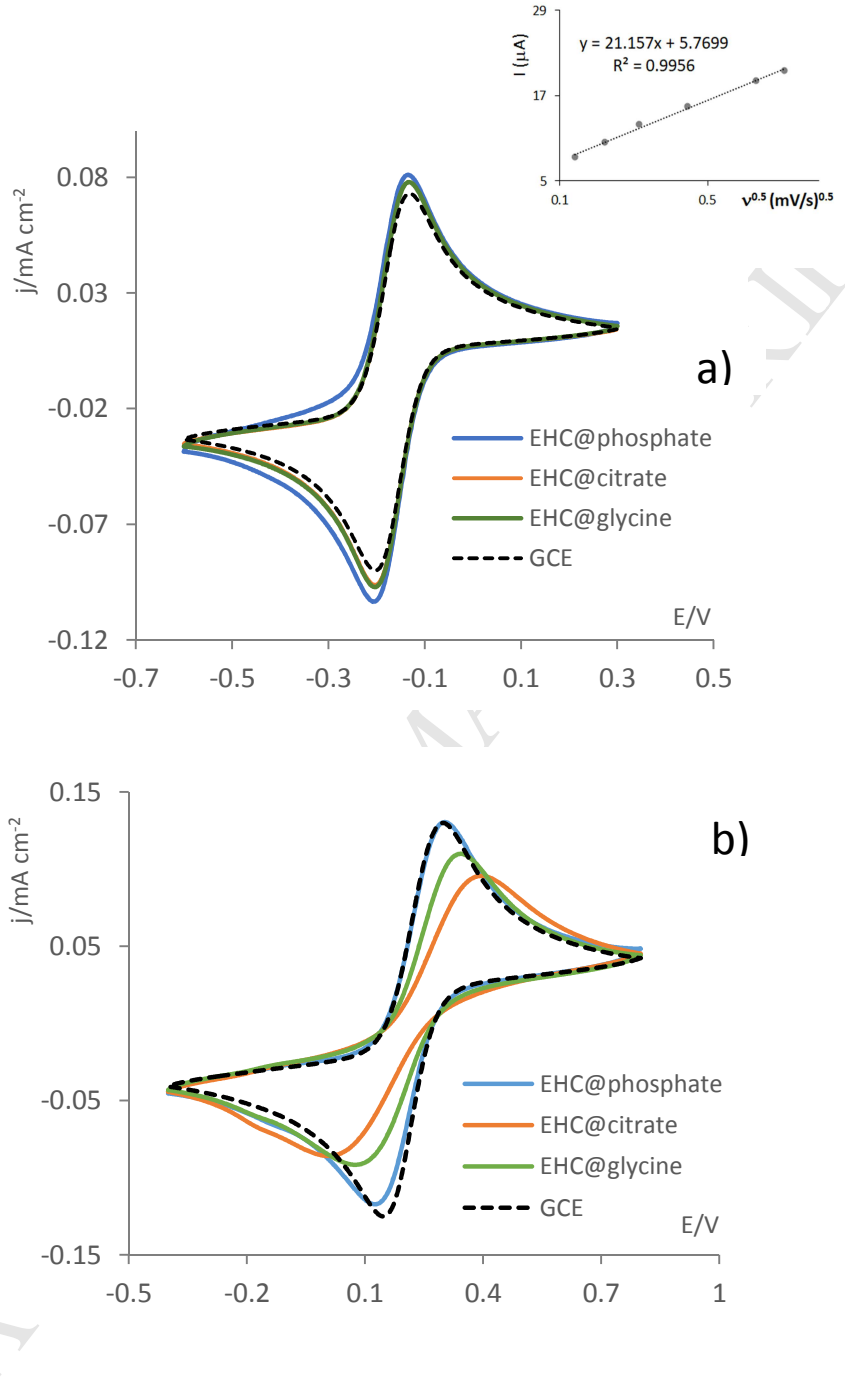
y = 21.157x + 5.7699
R² = 0.9956
I (µA)
29
17
5
0.1
0.5
v^0.5 (mV/s)^0.5
j/mA cm-2
0.08
0.03
-0.02
-0.07
-0.12
-0.7
-0.5
-0.3
-0.1
0.1
0.3
0.5
E/V
a)
EHC@phosphate
EHC@citrate
EHC@glycine
GCE
0.15
0.05
-0.05
-0.15
-0.5
-0.2
0.1
0.4
0.7
1
b)

Figure 4

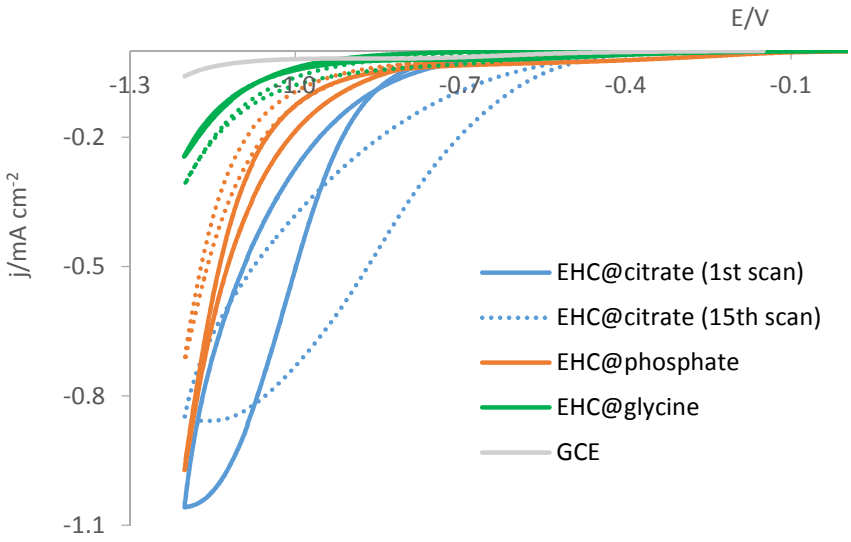

Figure 5

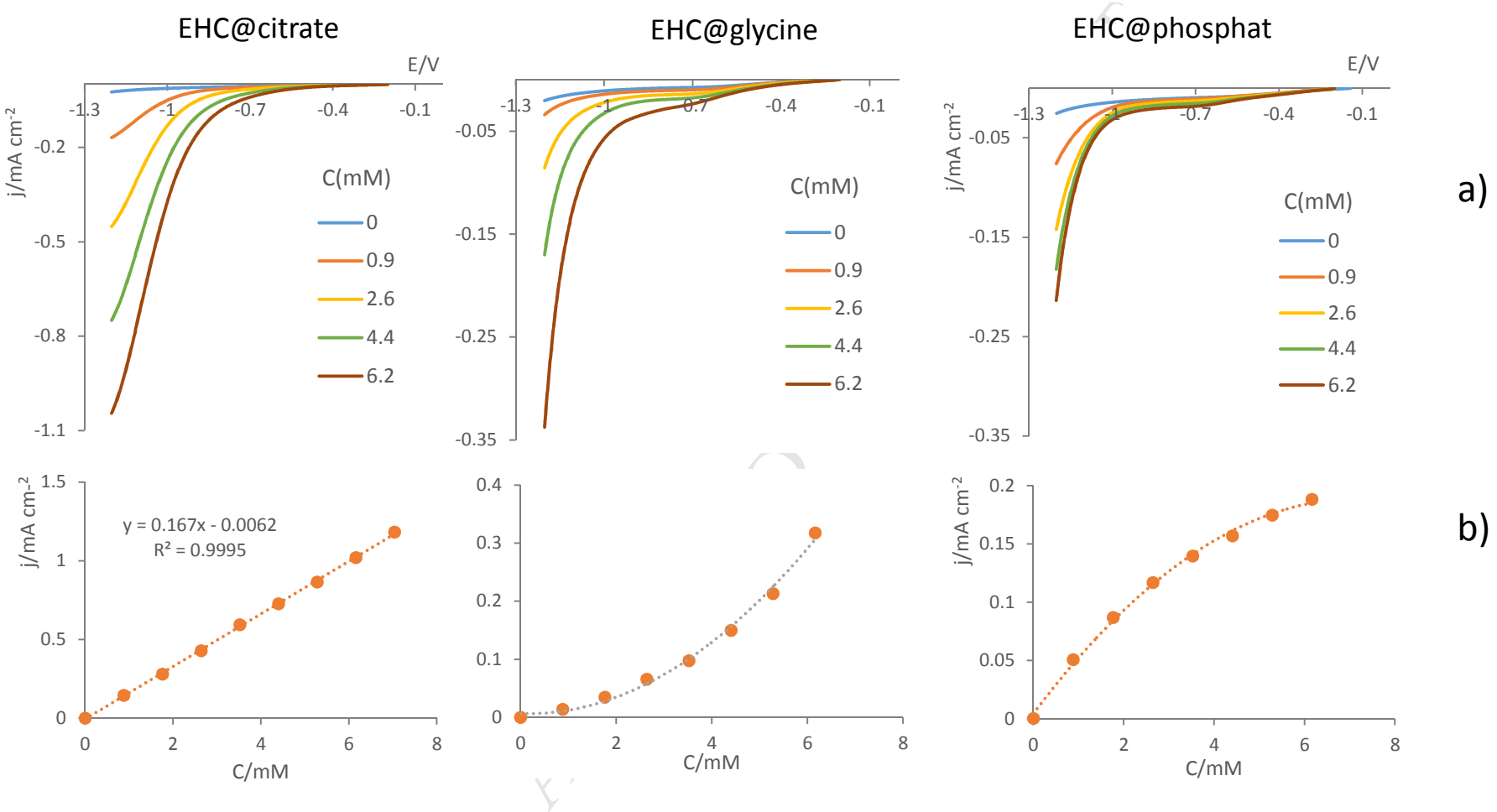
EHC@citrate
EHC@glycine
EHC@phosphat
E/V
j/mA cm-2
C(mM)
0
0.9
2.6
4.4
6.2
a)
y = 0.167x - 0.0062
R² = 0.9995
C/mM
b)

Figure 6

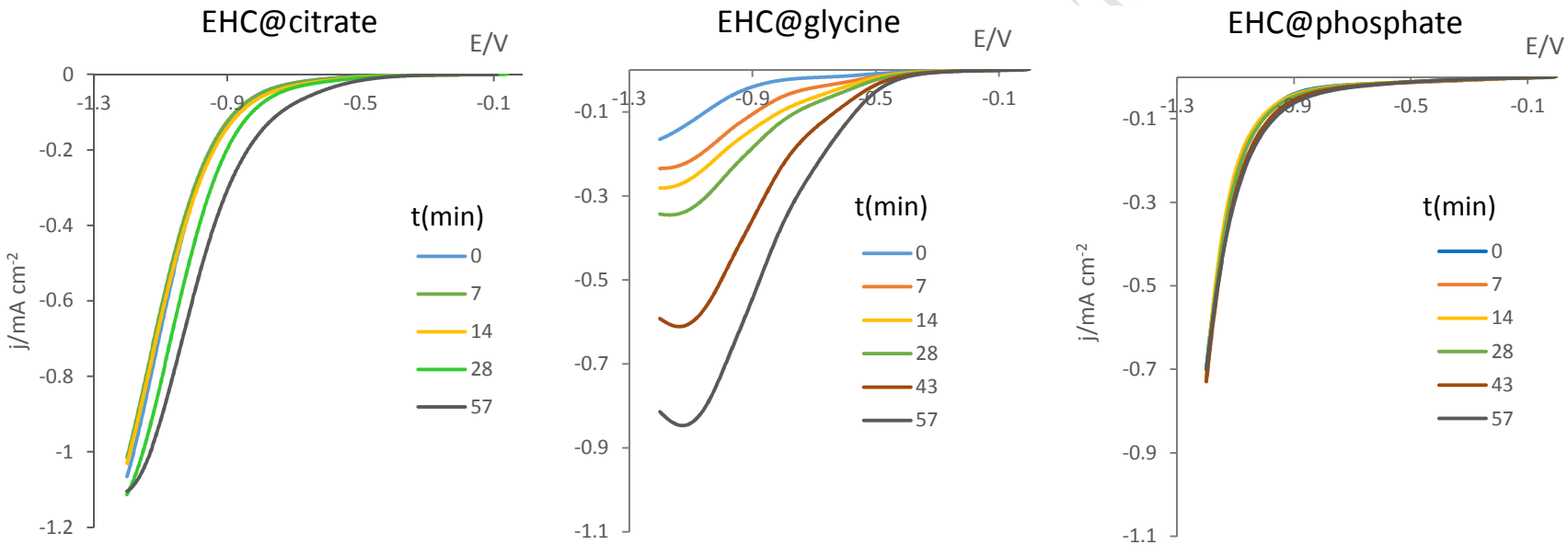

Figure 7

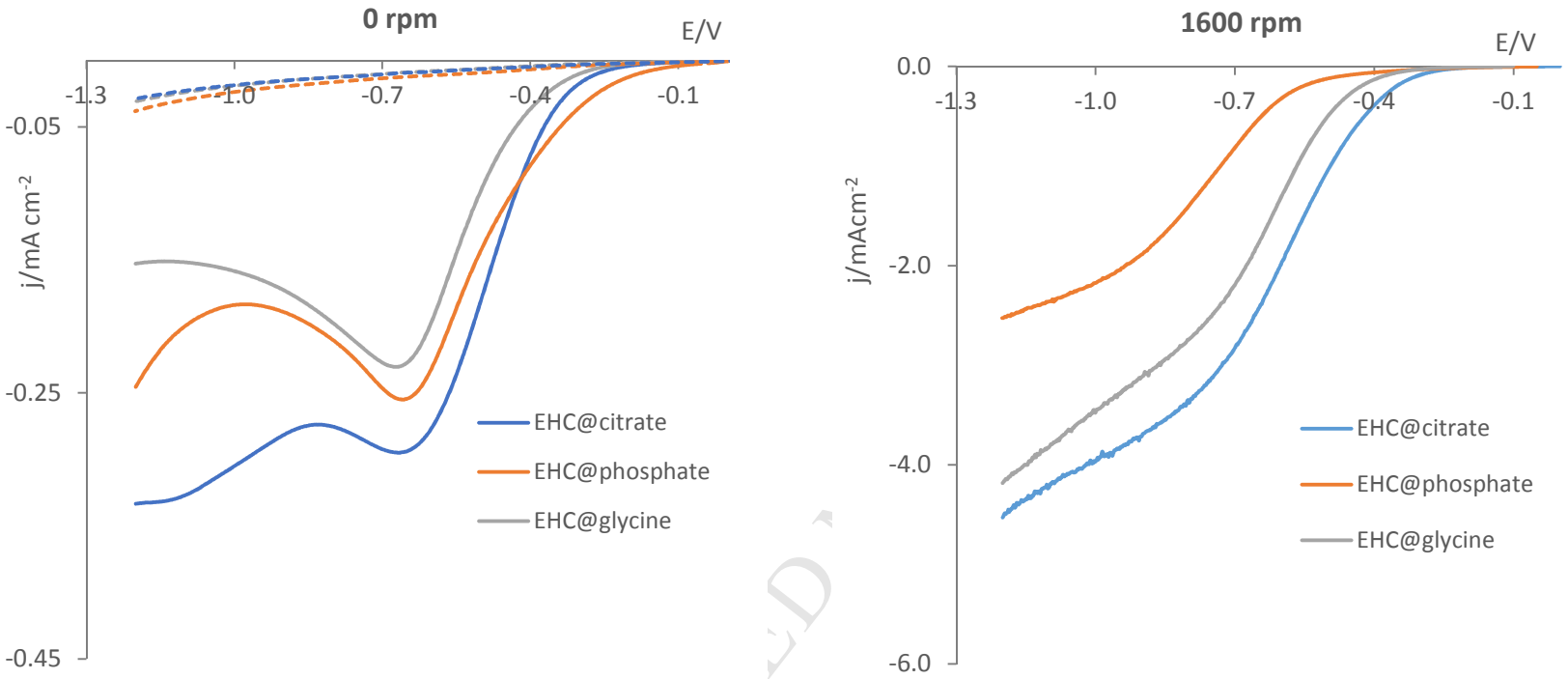

Figure 8

EHC@citrate

EHC@phosphate

EHC@glycine

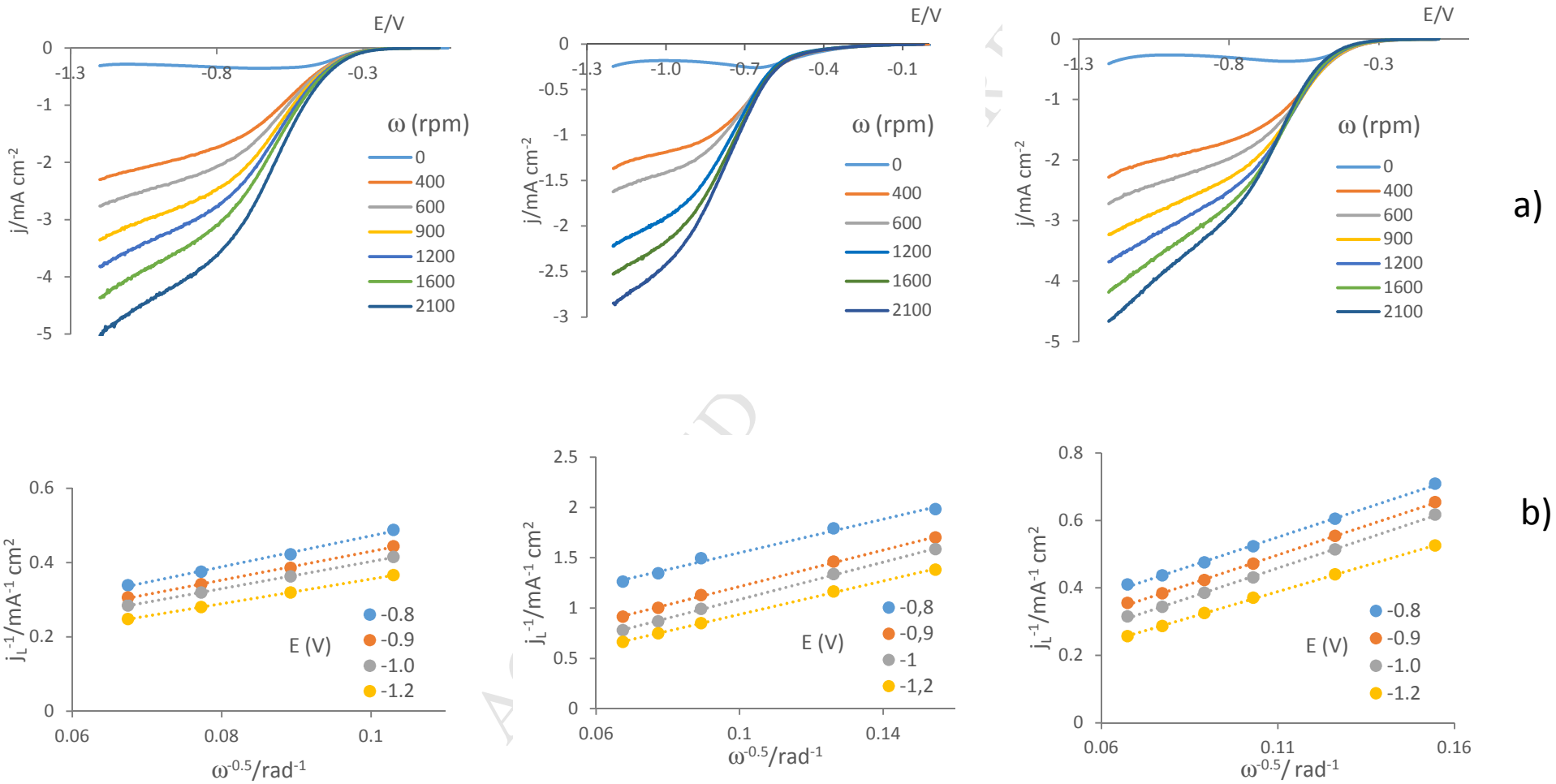

Figure 9

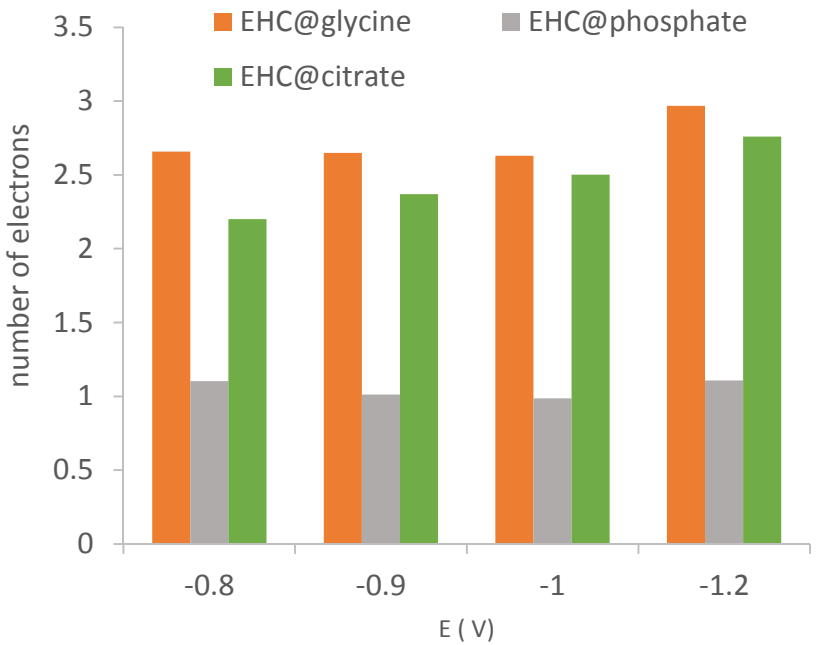
EHC@glycine
EHC@phosphate
EHC@citrate
number of electrons
3.5
3
2.5
2
1.5
1
0.5
0
-0.8
-0.9
-1
-1.2
E (V)

Figure 10

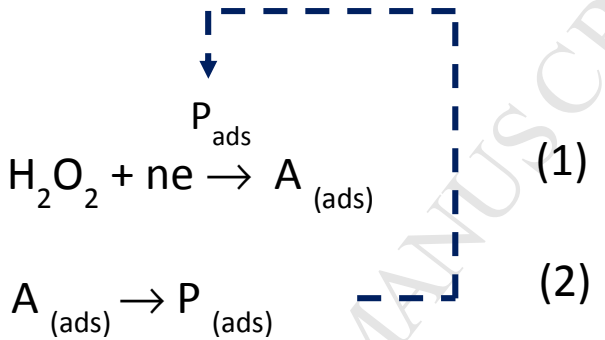

(1)

(2)

and $A_{(ads)} \rightarrow A_{(aq)}$ (3)

or/and $P_{(ads)} \rightarrow P_{(aq)}$ (4)

Figure 11

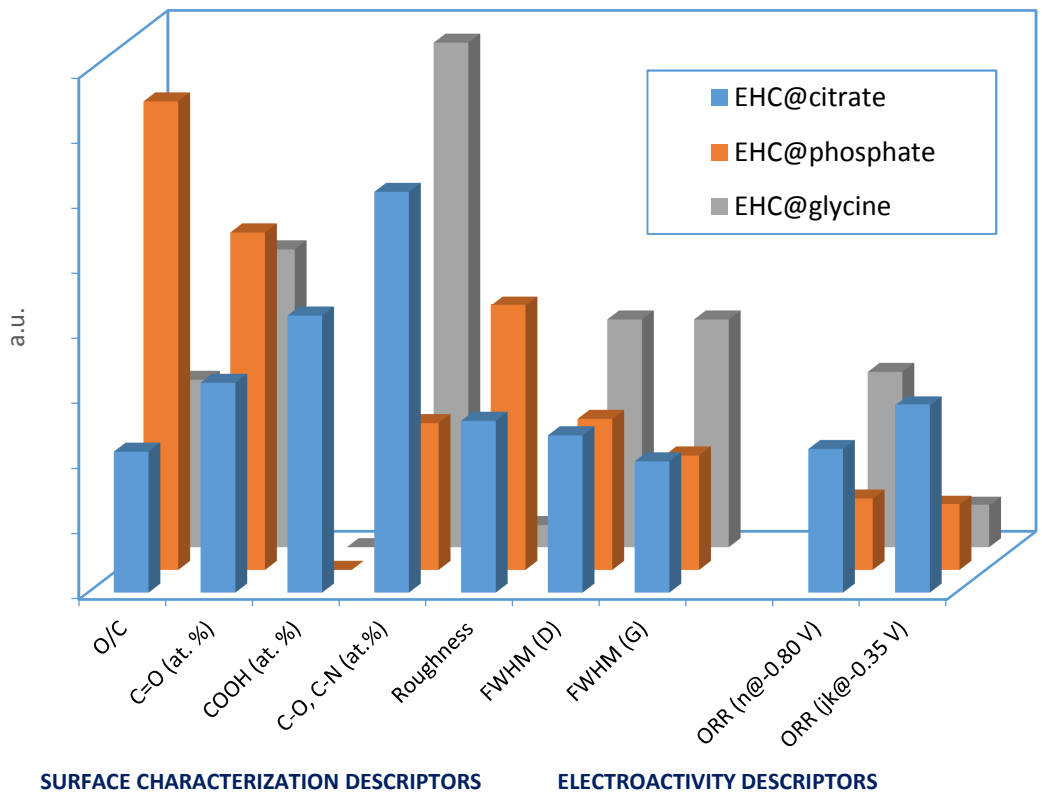
EHC@citrate
EHC@phosphate
EHC@glycine
a.u.
O/C
C=O (at. %)
COOH (at. %)
C-O, C-N (at.%)
Roughness
FWHM (D)
FWHM (G)
ORR (n@-0.80 V)
ORR (jk@-0.35 V)
SURFACE CHARACTERIZATION DESCRIPTORS
ELECTROACTIVITY DESCRIPTORS

Figure 12